FP6-2002-IST-1-002131

PICMOS

Photonic Interconnect Layer on CMOS by wafer-scale integration

STReP - Specific Targeted Research Project

IST – Information Society Technologies

D3.2 - Comparison of proposed architectures for µ-source and choice of design to be used for optical link

Due date of deliverable: M21 – Delivery: M22

Start date of project: January 1, 2004 Duration: 36 Months
Lead Contractor : CNRS Revision: Final
Contribution Partners: IMEC, CEA, TU/e

Dissemination Level: Public

Abstract

We report on the comparison of the different strategies for the integration of a photonic micro-laser on silicon, connected with a passive waveguide. All the different designs are briefly recalled, details are given on the design parameters, and state-of-the-art is discussed, both in terms of processing and performance. Based on considerations and results from WP1, we conclude that ultra-compact devices are much more suited than the semi-compact ones, as a basic building block for the final demonstrator. More specifically, we recommend using microdisks and DBR devices for the WP6 final demonstrator. This choice is made considering systems argument, technological maturity and first experimental results. However, for future application, more prospective devices could be considered.

Partner Contributions:
CNRS:

- Inputs from WP1
- Workpackage coordination
- Design and modeling of ultra-compact source
- Epitaxy for ultra-compact source
- Processing for ultra-compact source
- Characterisation of ultra-compact source

IMEC

- Design and modeling of ultra-compact source
- Processing for ultra-compact source
- Characterisation of ultra-compact source
- Design, fabrication and characterization of semi-compact source

CEA

- Bonding of epi for ultra-compact source

TU/e

- Epitaxy for semi-compact source

1. Introduction

In this deliverable, we present the different elements that can be considered in order to choose a laser concept to be integrated in the final PICMOS demonstrator. Up to month 21, five different architectures have been considered. Each one will be briefly presented in the following section, and the development status will be discussed. In section 3, we present the criteria that should be considered to select the most appropriate laser. This is mainly an input from WP1. The recommended laser architectures are also presented in this section. The recommended devices will be an input for WP6.

2. Status on the development of micro-laser sources

In this section, we describe the main features of each microlaser device that was investigated the PICMOS program. The devices are briefly described, and their expected (calculated) performances are given. The present status of the fabrication and available measured characteristics are recalled. A more detailed description of each of these devices can be found in D3.1 and its appendices.

2.1 Semicompact Fabry-Perot (FP) laser

2.1.1 Introduction

The goal of this work (semicompact laser) was to develop a laser with a footprint in the order of 1000um^2, which can be integrated with the waveguides developed in WP5 (SOI or SiN). Such a device is more comparable to standard lasers used e.g. for telecom applications than the ultra compact sources. The rationale for developing this laser is twofold:

- The ultracompact-lasers are limited in terms of maximum output power. For some applications (e.g. clock-distribution, inter-chip interconnect) larger powers (>1mW) may be required.
- Within the project, the semi-compact sources can serve as a backup if the ultra-compact sources fail.

2.1.2 Design and theoretical data

The laser designs considered here are more or less classic:

- **Transversal cross-section:** rather thick membranes are used (several micrometer) to avoid absorption in metal contacts.
- **Longitudinal cavity:** the fabrication scheme developed is compatible with well-known cavity types (Fabry-Pérot, DFB-like, DBR-like, ring-resonator).

Therefore, the main challenge of this work is to develop a reliable scheme to couple the light from the laser into the underlying waveguides. Different such coupling schemes have been studied:

- Evanescent coupling: although this scheme is used for the ultra-compact source, it can not be used for the semicompact source: the thicker cladding layers inhibit sufficient overlap of the laser mode with the underlying waveguides.
- Coupling through grating couplers: coupling efficiency is limited and very sensitive to variations in fabrication parameters. Therefore also this approach was ruled out.
- Adiabatic coupling through intermediate polymer type coupler (see Fig. 1). Coupling is very robust for process variations and rather efficient. The coupling scheme is compatible with both SOI and SiN waveguides. Several additional processing steps are required, which forms a potential drawback.

Because of its robustness, we have chosen for the third approach (coupling through intermediate polymer waveguide). This approach was described in detail in deliverable D3.1.

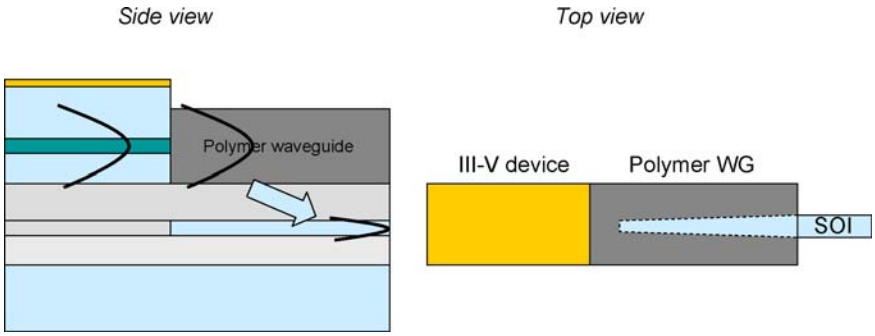

Figure 1 *Design layout of the coupling scheme for semi-compact laser diodes*

The laser design should be optimized for the application envisaged. For optimized fabrication conditions operation comparable to currently available commercial lasers could be obtained:

- Threshold current: 5-10mA
- Output power: several mW – External efficiency: 20%-50%
- Modulation speed: ≤10GHz (limited by size of device)

To obtain the power coupled into the actual waveguide, the laser output power has to be multiplied by the coupling loss. This coupling loss is around 2dB taking into account current fabrication limitations. We estimate improved design can lower this to 1dB.

2.1.3 Fabrication status and experimental data

- Bonded Fabry-Perot lasers have been fabricated. Pulsed laser operation was obtained. Lasers are very sensitive to heating because of the intermediate bonding layer. Appropriate heat-sink has to be designed.
- Coupling light from SOI-waveguides to polymer waveguides has been demonstrated. Loss was estimated to be 1dB.
- Facet etching process has been developed.
- Masks for integration of laser with both SOI-waveguides and SiN are ready.

2.1.5 Conclusion

Semicompact sources can be useful for applications where higher output power is required. This will of course also require higher input power (higher driving current). Compared to the ultra-compact source, the modulation speed is limited by the size of the device.
With regard to the fabrication: all processing steps have been separately developed and are ready for integration. First complete integration of laser + coupler + waveguide is expected for January ’06.

2.2 Distributed Bragg Reflector (DBR) microlaser

2.1.1 Introduction

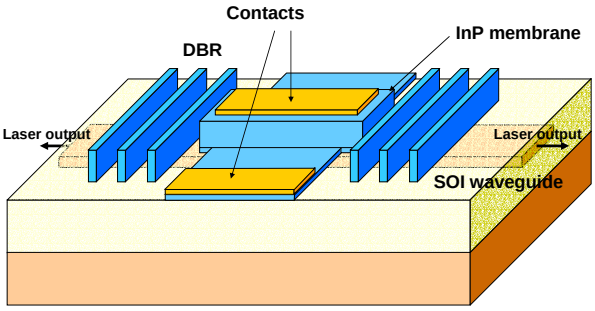

Figure 2 *General layout of the membrane DBR-microlaser*

The DBR-microlasers developed here consist of a ridge waveguide terminated with DBR-mirrors on both sides, defined in a III-V membrane. These devices can be fabricated on top of an SOI-waveguide wafer (Figure 2). Laser cavity losses include contact metal absorption loss, absorption losses in doped semiconductor layers, DBR-leakage and useful emission into the SOI-waveguide.
The footprint of this device is some 100µm² (20 to 40µm long, around 10µm wide), and the device is expected to exhibit a high bandwidth. Since the device is based on a thin III-V membrane bonded onto silica, evanescent coupling of light to SOI waveguide has been considered.

2.1.2 Design and theoretical data

The internal laser cavity losses depend strongly on the specific epistructure design. Absorption can occur at the metal contact as well as in (heavily) doped semiconductor layers, which are needed for electrical injection. In order to minimize this loss, we performed an optimization of these losses, for four different epistructure designs, which should all be compatible with efficient electrical injection: in a first approach, we use a conventional p-type contact, in a second we use a tunnel junction (TJ). For both designs, we studied the influence of the position of the p-type layer or the TJ in the epistructure (top or bottom). TJ or p-type contacts on the top of the membrane are preferable as far as modal loss is concerned. The influence of the III-V membrane global thickness has also been studied. The outcome is that it with a thickness over 1µm, modal losses can be kept below 20/cm.

However, as far as epitaxial growth is concerned, p contacts should be positioned on the bottom of the heterostructures and the thickness should not be too high in order to maintain evanescent coupling between the laser and an SOI waveguide. Finally, in this framework, we used an epistructure with a TJ in the top, and with a thickness t in the 750-1000nm range.

We performed a two-dimensional eigenmode expansion analysis in cross-section of the complete DBR microlaser, using the CAMFR software tool. This analysis, performed in the case of a TJ on the top of the epistructure, yields the threshold material gain in the four quantum wells, as well as the coupling efficiency into the SOI-waveguide. The bonding layer thickness d was chosen to be 200nm.

- For t = 750nm, material gain threshold levels are in the range 1000-2000/cm for cavity lengths ranging from 10 to 40 µm. These values are compatible with physical gain levels in compressively strained quantum wells. The coupling efficiency η_{extr} ranges

from 0 to over 20%. Since we had to increase the membrane thickness to reduce absorption losses, many guided modes can be excited, and we find a peak in the laser threshold gain when they interfere destructively.

- For t = 1000nm, material gain threshold levels are lower: in the range 600-1600/cm. This is due to the reduced modal absorption loss for thicker membranes. Coupling efficiencies η_{extr} are also higher (0-30%). However, the interference effect with higher order modes becomes more important, since there are more higher-order modes available (with lower modal loss). Choosing a thicker membrane thus can reduce threshold gain levels, but makes fabrication more difficult.

From the above modeling results, we can try to estimate the threshold current density I_{th}/W (W = ridge width) and slope efficiency η_{slope} of the DBR-microlaser. The results as a function of cavity length are given in Figure 15, for t=750nm. For a cavity length of 18µm, the resulting I_{th}/W-values are for a loaded cavity (with a SOI waveguide underneath) around 520µA/µm, with a slope efficiency of about 0.1mW/mA. These values of course assume perfect fabrication, and laser emission is bidirectional in the SOI-waveguide. These simulations also don't include radiation losses in the third dimension, which might get important for small W, thus causing a larger I_{th}/W-value and a smaller η_{slope}.

2.1.3 Fabrication status

Currently, three samples with DBR-microlasers were processed (without underlying SOI-waveguide). The specific fabrication process involves e-beam sub-micron lithography, transfer to the SiO_2 hard mask and etching of the DBR-structures. The DBR target parameters were 550nm for the period and 180nm for the slit width, without any sidewall slope. The results of the fabrication efforts (with RIE-etching method) are depicted in Fig. 3. From these images can be seen that the mirrors have some roughness and a sidewall slope of more than 5 degrees. It is clear that at this point our current process doesn't meet the required specifications.

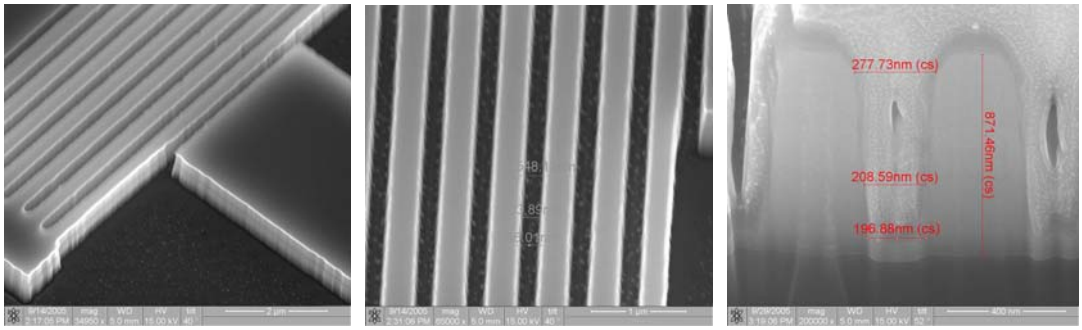

Figure 3 *SEM-pictures of DBR structures*

2.1.4 Test status and experimental data

The quality of the fabricated DBR-microlaser cavities was tested by means of micro-photoluminescence. Cavities with lengths of 15 and 30µm and widths of 3 to 8µm were available. No optically pumped lasing was observed. However, for the biggest structures, some resonant features with a maximum quality factor of 300 could be distinguished in the micro-photoluminescence spectra (see figure 4). We conclude that the quality of the DBR-mirrors is at this point not good enough to yield laser resonance.

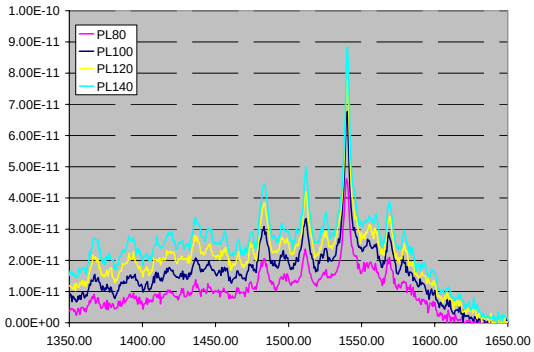

Figure 4 *Micro-photoluminescence spectrum of a 30x8μm^2 DBR-microcavity*.

2.1.5 Conclusion

Two-dimensional modeling results suggest that perfectly fabricated DBR-microlasers coupled to an SOI-waveguide can support laser modes with a current density threshold I_{th}/W around 520µA/µm, and with a slope efficiency of about 0.1mW/mA (cavity length = 18µm). For a typical cavity width of 3µm, this would result in a current threshold of 1.5mA. First samples with DBR-microcavities have been fabricated using e-beam lithography and RIE-etching. At this point, the process doesn't meet the required specifications. Micro-photoluminescence measurements indicate that the microcavity quality is not good enough to reach laser resonance. The quality of the cavity can be improved by reducing the sidewall slope of the DBR-mirrors. This requires a better fabrication process.

2.3 Two-dimensional photonic crystal (2DPC) microlaser

2.1.1 Introduction

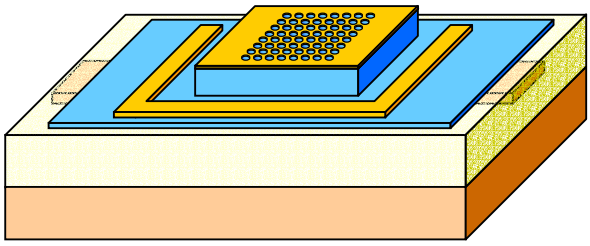

Figure 5 *Electrical injection schemes for the two-dimensional photonic crystal (2DPC) microlaser*

Current state-of-the-art membrane optically pumped microlasers also include two-dimensional photonic-crystal (2DPC) microlasers, based on the band-edge resonance effect. They are typically fabricated in monomode membranes, which are quite thin (<300nm) due to the high vertical index-contrast. Since these structures exploit in-plane guided resonance, and because they are based on a thin III-V membrane, evanescent coupling can be used, similarly to DBR lasers.

Two electrical injection schemes were considered. In the first scheme, a metal contact is placed on both sides of the membrane, and only surface emission is possible. Indeed, due to the bottom metal contact, coupling to an underlying waveguide is not possible. The second is analogue to the electrical injection scheme of the DBR-microlaser: the bottom contact is placed next to the cavity on a thin contacting membrane. Then light can be coupled evanescently to an underlying SOI-waveguide. This last scheme should be preferred to build

the final optical link. As in the DBR case, the main difficulty consists in using a membrane about 1µm thick and meanwhile to reduce the influence of higher order guided resonances. Lastly, one should note that the top contact is positioned on the whole InP surface, all around the holes, which is a strong technological constraint.

2.1.2 Design and theoretical data

The influence of the metal contacts and the multimodality of the membrane on the photonic crystal resonance were studied for the first electrical injection scheme, in a two-dimensional cross section, with the CAMFR software tool. The simulation results reveal that for a membrane thickness of 1µm and a cavity length of 30µm, this kind of structures can support resonances with a quality factor of about 2500. In this case about 20% of the total cavity loss is due to (useful) surface emission. Coupling to lossy higher order modes needs to be avoided, by a proper design of the photonic crystal. Nevertheless, metal losses are very high, consuming about 70% of the total cavity loss.

The multimodality of photonic crystal resonators based on a 1µm thick III-V membrane was investigated by plane wave expansion simulations (MPB software). The membrane are surrounded by silica, and the simulations were performed for the three guided modes that can be supported by the membrane : mode 1 (3.13 effective index), mode 2 (2.93 effective index) and mode 3 (2.57 effective index). We assume in these simulations that the lasing mode is the mode 1 (fundamental). The influence of mode 2 is considered negligible, due to its odd parity. Mode 1 and 3 are even and a coupling is possible and can affect the resonator quality factor.
Simulations have been done on triangular and graphite lattice 2DPC membranes. In both cases, we considered all the low-group velocity modes at the vicinity of the Γ-point, as well as around the K and M-points, the gap between such resonance corresponding to mode 1 and 3 exhibit a gap of more than 100nm. This means that only one resonant mode could lie within the optical gain spectral range. Therefore, the multimodality should not imply resonant modes competition mechanism.

2.1.3 Fabrication status

The main difficulty consists in drilling 1µm deep circular holes into the InP membrane. The problem is then similar to DBR-like resonators, the shape of the holes should be well controlled in order to enhance the final quality factor. The fabrication procedure is otherwise similar to DBR-lasers. So far, the sidewalls slope is more than 5°, using RIE, which is too important. The development of this process would need to allocate more manpower on etching development related tasks.

An important fabrication aspect of this kind of devices is the ability to deposit a metal contact on top of a photonic-crystal pattern, *without* filling the holes. Some preliminary tests involving oblique evaporation were performed with good results (see Fig. 6).

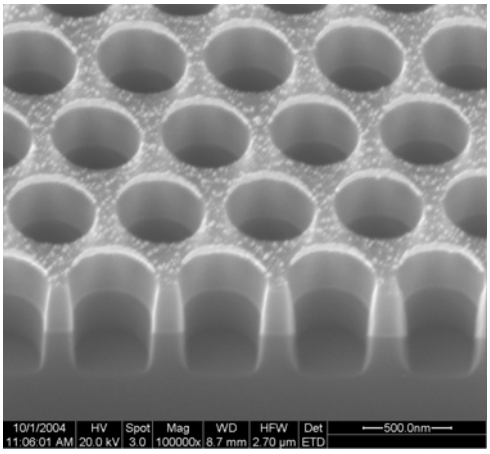

Figure 6 *Oblique gold evaporation on a photonic crystal pattern*

2.1.5 Test status and experimental data

Due to the impossibility to achieve the hole etching with perfect vertical walls by means of RIE, the fabrication of the 2DPC microsources has been postponed.
The close control of the hole etched depth needs also to be addressed, in order not to degrade the electrical properties of the bottom contact layer.

2.1.6 Conclusion

2DPC low-group velocity modes are well adapted for the fabrication of ultra-compact microlasers, due to their reduced footprint (some 100µm²) together with their high Q-factor. However, the fabrication procedure is more complex than the semicompact and DBR lasers, and there are no experimental results at the present time. Moreover, the structure is basically 3D, and it is complex to simulate its global behavior, this is why only modeling elements are exhibited here.

2.4 Diffractively coupled (DC) microlaser

2.4.1 Introduction

These structures exploit a laser resonance that has a complex nature. It is both a "vertical" resonance, like in a VCSEL, and a guided resonance, like in a photonic crystal laser. The footprint of these structures is of the same order as that of 2DPC structures (see Fig. 7). The coupling scheme is different, and is purely diffractive.

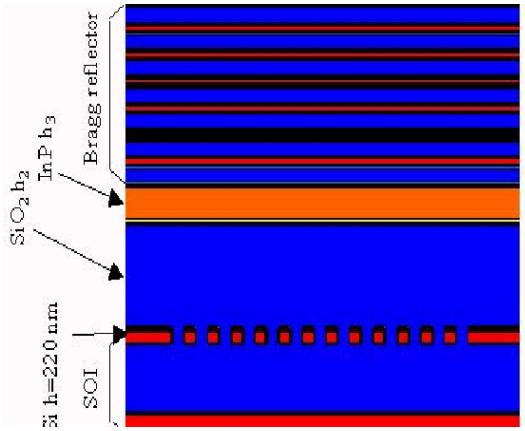

Figure 7 *Cross section view of a diffractively coupled microlaser*

In such lasers, both a planar photonic crystal and a vertical Bragg reflector are necessary. The idea is to pattern the photonic crystal in the SOI layer, thereby exploiting silicon related technological processes, and to position the InP-based gain layers on top, then it is no more necessary to pattern it. This alternative makes it possible to exploit a relatively standard electrical injection scheme (large metallic contacts on an InP heterostructure without PhC holes). The thin silicon layer of the SOI wafer is then both a part of the resonator (where it is patterned as a PhC), and of the output waveguide (where it is not patterned).

2.4.2 Design and theoretical data

This device was designed during the first year of the program. These resonators should include a 220 nm thick silicon PC layer, as it corresponds to the IMEC technological standard for SOI. Optimisation was performed in order to increase the Q factor, and to adjust the lasing wavelength. The best compromise was found for a 1D PhC (slits) patterned in the silicon layer of the SOI, with a 850nm lattice parameter. The silica and III-V heterostructure thicknesses are respectively around h_2=1400nm and h_3=500nm. Q factors as high as 3500 should be achievable. This is lower than the ~15000 value that is obtained if the technological constraint on this Si layer thickness is eliminated, but still enough to perform laser emission. The influence of technological inaccuracies (bonding layers and epi-layers thicknesses) was studied. It was demonstrated that, with a +/- 5% thickness fluctuation, the Q factor should remain over the 1000 regime.
In this scheme, the optical coupling of light to Si waveguides has also been simulated. We calculated by 3D FDTD that at least ~20% of the light could be coupled to the Si waveguide that stands beside the silicon 1D PhC structure.

2.4.3 Fabrication status

SOI pre-structures were generated in IMEC along the simulations that were performed in CNRS. The subsequent device fabrication was postponed.

2.4.5 Conclusion

This laser design has a strong potential provided the constraint on the silicon photonic crystal thickness is eliminated. It could enable in the same time an efficient coupling and benefit from a very high quality factor. The electrical injection scheme is more classical than in the 2DPC and microdisk cases.

2.5 Microdisk (MD) lasers

2.5.1 Introduction

Laser microsources based on microdisks have been fabricated, with the advantage of using only UV photolithography, compared to 2DPC or DBR lasers, where e-beam lithography is needed. On the other hand, the rest of the technological process is similar to DBR fabrication : a side contact, a localized top contact and a tunnel junction are used. This bottom contact layer is obtained by a partial RIE etching of the structure, during the disk etch process. The depth etch is controlled by reflectometry. The microsource design is shown in the Fig. 8.

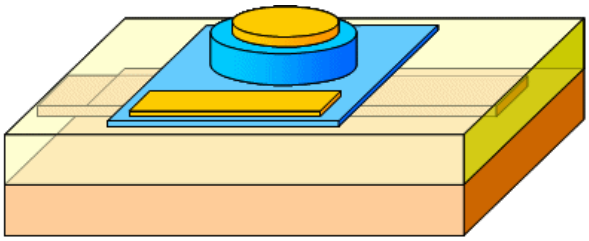

Figure 8 *Microdisk laser design*

The footprint is limited since the microdisk itself is around 5 to 10µm in diameter. Moreover, these devices are quite well suited to evanescent coupling to SOI waveguides since the resonant mode are "whispering gallery modes", which electromagnetic field localization is quite similar to that of SOI wire waveguides.

2.5.2 Design and theoretical data

The main parameters that drive the lasing characteristics and the optical coupling efficiency to SOI waveguides are (1) the membrane thicknesses (we used : 0.5 and 1 micron membranes) and the SiO_2 bonding layer thickness.

The influence of the bottom contact semiconductor slab was evaluated, in terms of optical losses. The presence of this membrane may reduce the quality factor Q of the microdisk to a value too low to allow a lasing operation. 3D Finite Difference Time Domain (FDTD) simulation were performed on 2 µm radius disk with a thickness h of 0.5 and 1 µm, and varying bottom slab thicknesses h_s : 0, 50 and 100 nm.
We found out that, for a 0.5 µm thick microdisk, the quality factor will be limited to Q~15000 with a 50 nm bottom slab, and to Q~10000with a 100 nm bottom slab. For a 1 µm thick microdisk, the quality factor will be limited to Q~20000 with a 50 nm bottom slab, and to Q~10000with a 100 nm bottom slab. However, in case of coupling between several vertical modes quality factors will be smaller, even without bottom slab, and the influence of the slab, in terms of losses, will be stronger.

Finally, it seems the best choice to exploit the purely whispering gallery mode referred to as (0,0,20), with a 50 nm bottom contact slab layer thickness, either with a 500 nm or a 1 µm global microdisk thickness. The bottom semiconductor contact slab should not be too thin in order to prevent an increase of the series resistance, leading to a device temperature increase that may impede lasing operation.

2.5.3 Fabrication status

The fabrication procedure includes partial RIE etching with interferometric control, BCB planarization and metal contacting (figure 9). The microdisk lasers were fabricated without any Si wave guide below the III-V layers.

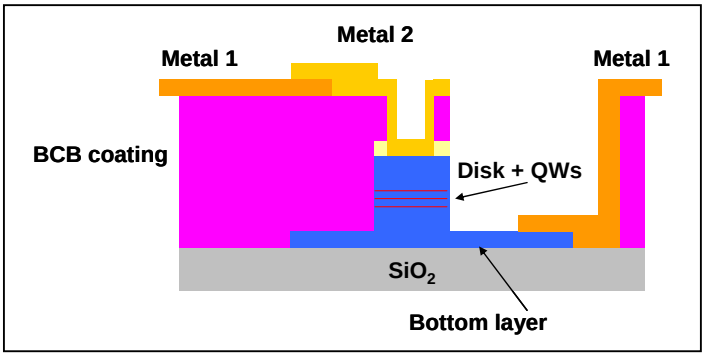

Figure 9 *Microdisk source fabrication*

2.5.4 Test status and experimental data

From static I-V measurements, a series resistance up to 300 Ω was extracted. This value, due mainly to the influence of both tunnel junction and bottom slab resistance, has to be reduced for a satisfactory laser operation.

For the optical characterization under electrical injection, a specific set-up has been developed. Electrical signal are provided to the sample using K. Zuss probes. For DC analysis a HP4145 is used. For pulsed signal injection, we use a Tektronix PG501 pulse generator and a HP power splitter. Light emitted by the microdisk is observed with a linear IR camera. For spectral characterization, light is collected by a lensed fibre close to the microdisk (50 nm precision positioning) and analysed by a J.Y Triax 550 monochromator.

The lasing operation on a 8 µm diameter disk is shown in the Fig. 10. The injection signal is a 6 ns pulse at 3 MHz.

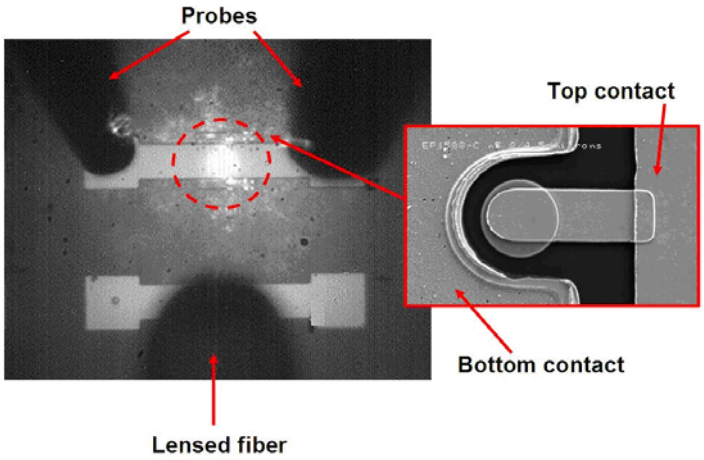

Figure 10 *Microdisk laser under test*

The Threshold current was determined at 1.5 mA, which corresponds to a 2.9 $kAcm^{-2}$ current density.
An important effort is being made to reduce this threshold current density : a better control of the doping levels during material growth, particularly for the tunnel junction layers, and improved designs for the bottom contact layer.

2.5.5 Conclusion

The design, fabrication and characterisation of these lasers could be achieved. The first results are quite encouraging although the lasing threshold should be reduced. It appeared that this design, although it could seems complex (the behaviour is purely 3D), ends up to be quite straightforward since whispering gallery modes are well known.
The processing complexity of such lasers is limited since it does not necessarily imply the use of electron-beam lithography. However, the development of the electrical injection scheme is the result of a long term effort that includes the development of dedicated tunnel junction heterostructures, low loss metallic contacts design.

3. Choice of the devices to be inserted in the final link demonstrator

In this section, we discuss the choice of the lasers that will be integrated in the final link demonstrator. In this part, we benefit from inputs from WP1 concerning the criteria for the laser selection.
We will consider arguments for selections in two different contexts:

- The choice of a device for the final application should consider the *final* properties of the lasers, which will be obtained after full development of the fabrication procedure.
- The choice of the laser that will be used within the project. The properties of the devices obtained at the present time, including design, fabrication results and experimental results are then of prime importance.

One should note that the selection in these two different situations will not be necessarily similar. Indeed, devices that exhibit high potential performance, but that need strong effort of the fabrication procedure development should be considered for medium-long term applications.

Criteria for selection of a source in the framework of optical interconnects are the following:

- compactness (impact on achievable interconnect density)
- bandwidth (impact on achievable data rate / power ratio)
- efficiency (impact on power dissipation)
- threshold current (impact on power dissipation)
- temperature dependency (impact on reliability)
- minimum output power

As all devices are designed to achieve bandwidths of 10GHz or greater, this criterion will not be considered for the selection. As compactness is intrinsically linked to the bandwidth, small devices will compare favourably to larger devices in the long term choice (clock frequencies higher than 10GHz are predicted by the ITRS for the 57nm technology node in 2008 for printed gate lengths of 32nm, as shown in Figure 11).
More contextual criteria consist of the feasibility of the device in the short term for the overall success of the project, and the number of degrees of freedom each device offers to optimise optical interconnect performance.

These criteria have been summarized in the following table for each considered source device. In this table, expected values of coupling efficiency and threshold current are given.

Device		Feasibility (A High – E Low)	Minimum footprint (with contacts)	Coupling efficiency to Si waveguides (estimated)	Threshold Current
Semi Compact		A	100umx100um	80%	Few mA
Ultra Compact	DBR	C	10umx30um	35%	100-200μA
	MicroDisk	B	10umx10um	25%	10-100uA
	2DPC	D	10umx10um	25%	100uA
	Diffractively coupled	E	10umx10um	20%	100uA

The values of threshold current measured on the first devices fabricated is significantly higher that the expected values indicated above for two reasons : (1) the technology is not mature and (2) the contact design for isolated devices includes wide contacts for probe testing, which increase artificially the contact resistivity.
At the present time, no data is available for temperature dependency of the devices and for internal efficiency of the lasers.
Considering these criteria, it appears that the semicompact source is not a good choice. Since, based on input from WP1 and in view of the envisaged application (point-to-point links) only limited output power is needed, its main advantages (high feasibility and good coupling) are outweighed by a high threshold current (which negatively compensates the coupling figure as concerns power dissipation) and low compactness (negatively impacts the achievable interconnect density).
This is shown in Figure 12, which compares the achievable number of links per optical channel for varying processor numbers (calculations were carried out for a single row of processors; the calculations still hold when extended to a processor matrix). The total chip size was assumed to be 20x20mm and the processors of identical sizes. Waveguide pitch was taken as 1.1um. Source and detector staggering was used whenever necessary. Optical link channels were considered to be used for all inter-processor communication. It is possible to improve on these figures by not routing optically between physically adjacent processors (electrical buses used in this case), and/or by defining a minimum length above which routing is done optically, but in a first approach the basic figures are given. Following transistor-level synthesis of the interface circuits under worst case conditions, the total gate area of these circuits was calculated (modulator and bootstrap total 2.7um^2 gate area in 65nm technology for 20mm link length, source threshold current set at 1mA and responsivity at 10%) and the total circuit area estimated from this, including via stack area (=15um^2 for 5mA maximum source current). They were found to be in all cases considerably less than that of the active device (i.e. the active devices remain the limiting factor for area concerns rather than interface circuits).

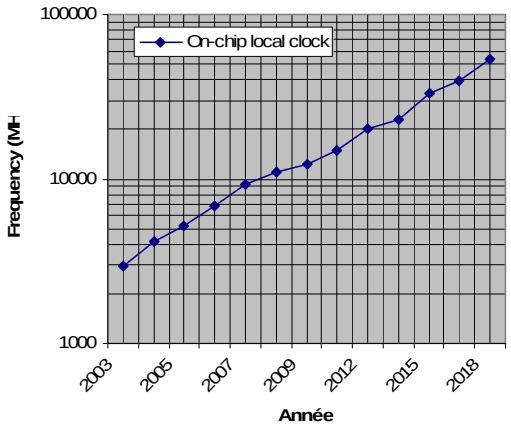

Figure 11 *On-chip local clock frequency predicted by 2003 ITRS*

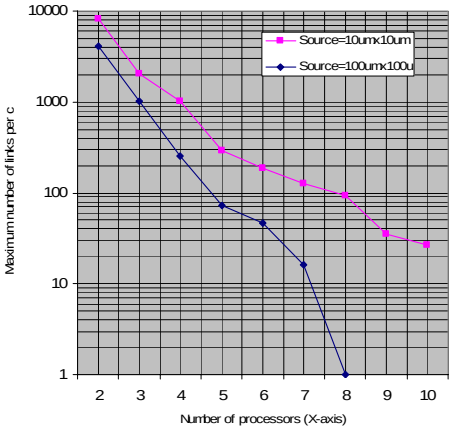

Figure 12 *Maximum number of links per optical channel with respect to number of IP blocks to interconnect and source size*

In terms of power, the maximum static dissipated current at the emitter was calculated for varying link lengths (from 2.5mm to 2cm) and source threshold currents (10uA, 100uA and 1mA), shown in Figure 13. The calculations were based on achieving 10uW difference in received optical power (sufficient to guarantee link BER<10^{-15} in worst case noise conditions for photodetector and receiver circuit) and considering waveguide attenuation at 2dB/cm, and source efficiency at 0.1mW/mA. The figures for aggregated maximum number of links per optical channel and associated channel lengths (including additional length due to device staggering) were then used in conjunction with the static current dissipation figures to calculate the total static dissipated current in one row of totally interconnected IP blocks, for varying number of IP blocks (from 2 to 10) and source threshold current (Figure 14). Relating this to the most long-term technology node (18nm in 2018, printed gate length 10nm), this gives a total power of I_{1row} * $2N_{processors}$ * 0.7V : for a 10x10 matrix of IP blocks this gives 58.8W, 8.4W and 3.4W for source threshold currents of 1mA, 100uA and 10uA respectively. Comparing this to the figure given for maximum power at this technology node (300W), these figures work out to 20%, 3% and 1% of total power for emission alone (receiver power represents a further contribution).

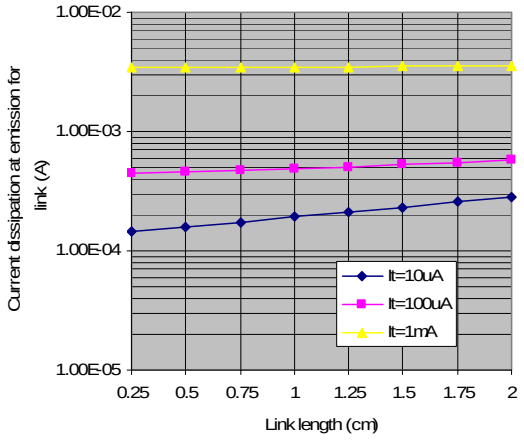

Figure 13 *Current dissipation in emitter circuit (modulator and bias) for varying link lengths and source threshold current*

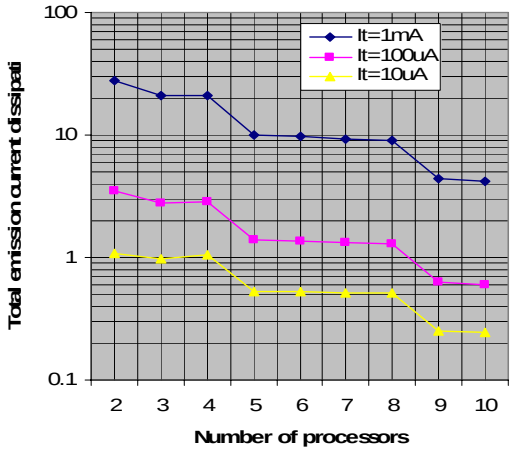

Figure 14 *Total current dissipation in emitter circuits for varying number of interconnected IP blocks (one row only) and source threshold current*

Concerning the choice between the various ultra compact sources, the 2DPC can be eliminated as being the device with highest risk while not offering significant advantages in terms of overall performance. Diffractively coupled source could be considered for long term applications, but it needs a strong effort to develop its processing.
It has been decided that although the Microdisk source is probably the best choice over the DBR source in terms of performance these two designs will be considered. However, the DBR source allows for more degrees of freedom in its design (Q factor, number of resonant modes), and their global properties have been calculated more precisely. Hence it is recommended that work continues on both sources. Thus, in the event of the microdisk source showing as yet unforeseen design limitations, a backup solution in the form of the DBR source will be available.

4. Conclusion

As far as optical interconnect related criteria are concerned, and considering in the same time the state of the art of the possible laser architectures, we selected microdisks and DBR lasers as possible basic components for the final link demonstrator. They are the most compact devices; they are compatible with high bandwidth and low threshold operation. This choice was made on the basis of available experimental data and theoretical prediction. Work on WP3 will be continued during year 3. In particular, the goals are to obtain en experimental determination of the coupling efficiency for the selected designs, and to stabilize the electrical injection technology (D3.3). By the end of this project, final sources characteristics will be considered by WP1 partners to update models and specifications (D1.3).
Therefore, we allocated more resources on microdisks and DBR lasers during the year 2.
For longer term applications, more prospective approach like diffractively coupled sources could be considered, the development of these sources could then be considered in another framework.